PAPER

Nanostructured ZnO thin films for self-cleaning applications

Mohamed Shaban,* Mohamed Zayed and Hany Hamdy

Controlling the properties of nanostructured zinc oxide (ZnO) is an interesting way to broaden its multifunctionality. ZnO nanostructured films were grown on glass substrates under different conditions by a simple two-step wet chemical method. A low-cost successive ionic layer adsorption and reaction (SILAR) method was used to grow ZnO seed layers at 80 °C. Then, different hierarchical based ZnO nanostructured thin films were deposited onto the ZnO seed layers by chemical bath deposition (CBD). The influence of deposition time (t_D) and pH on the surface morphology, wettability behavior, structural and optical properties of the ZnO nanostructured films were systematically investigated. The structural, morphological, optical and wetting properties were studied by X-ray diffraction (XRD), field emission scanning microscopy (FE-SEM), UV-Vis spectrophotometer, and water contact angle (WCA) measurement, respectively. The surface morphology revealed a complex and orientated hierarchical based ZnO nanostructured films with diverse shapes from hexagonal nanorods to hexagonal nanoplates and even much more complex plates/rods and flower-like shapes by changing deposition time and pH of the precursor. XRD results confirm the synthesis of nanostructured ZnO of the hexagonal structure with a preferential orientation along the (002) lattice plane. The average crystallite size, D, is altered between 41.41 to 68.43 nm dependent on the morphology of the ZnO film and pH of the precursor. At pH 6.5, the films are hydrophilic for 10 h $\leq t_D \leq$ 6 h and hydrophobic for 6 h < t_D < 10 h. The wetting properties of the films were enhanced by increasing or decreasing pH around 6.5. Morphology and thickness of the ZnO nanostructure could efficiently control the transmittance, absorbance, optical band gap, and the extinction coefficient of the films. The optical band gap is blue shifted from 2.45 to 3.62 eV@pH 6.5 as the deposition time increased from 2 to 8 h and blue shifted from 2.72 to 3.62 eV@8 h as the pH value increased from 5.5 to 6.5. The existence of stable hydrophobic zinc oxide nanostructured films at room temperature at a large-scale and with band gaps around 3.62 eV supports their use in self-cleaning and gas sensing applications.

1 Introduction

The wetting behavior of a film is a combined effect of its surface topography and microstructure, surface free energy, and the chemical composition.[1,2] In general, surfaces with water contact angle $\Theta \geq 90°$ are hydrophobic and those with contact angles $\Theta < 90°$ are hydrophilic.[3] The development of semiconductor (SC) metal oxide thin films of different morphologies with self-cleaning properties is one of the key technologies for opto-electronic applications. ZnO nanostructures exhibit strong spontaneous piezoelectric polarization because of their wurtzite structure, a hexagonal lattice in which the Zn^{2+} ions occupy the tetrahedral sites formed by the O^{2-} ions.[4] ZnO surfaces display better photocatalytic performance in the degradation of hazard dye molecules in both basic and acidic medium.[5] ZnO films

have thermal diffusivity in the range of $(4.35–5.03) \times 10^{-2}$ cm^2 s^{-1} and electrical resistivity varying from 10^{-4} to 10^{12} Ω cm.[6] The free exciton binding energy of ZnO at room temperature (RT) can be increased from 60 meV to >100 meV in super-lattices.[7] These distinctive physicochemical and optoelectronic properties of the transparent ZnO semiconductor material still stimulate enormous awareness for usage in a variety of industrial and technological applications. ZnO films are suitable for monitoring of some gasses like CO and H_2S and CH_4.[8] ZnO is considered as a next-generation light-emitting diode (LED) and room temperature (RT) polariton lasers.[9–12] ZnO film can be used as front contact material for dye-sensitized solar cells[12,13] because of its relatively high optical transmittance in the visible region and conductivity. Also, ZnO nanoparticles (NPs) were used in cosmetics and paints because of its ability to block the UV light.[14,15]

ZnO surfaces are generally hydrophilic (water contact angle $\Theta < 90°$).[16] The hydrophilic and superhydrophilic surfaces are used for practical applications such as antifogging and self-

Nanophotonics and Applications Lab, Department of Physics, Faculty of Science, Beni-Suef University, Beni-Suef 62514, Egypt. E-mail: mssfadel@yahoo.com; mssfadel@aucegypt.edu; Tel: +20 1274493440

cleaning.[17] However, hydrophobic and superhydrophobic surfaces can be used in many areas as antifouling, anti-icing, self-cleaning, and liquid transportation. Different approaches have been used to turned the ZnO surfaces from hydrophilic to hydrophobic.[18] UV illumination and long-term dark storage (or heating) are simple methods for the hydrophilic & hydrophobic transition. Also, doping and co-doping with specific elements is another way that could be used to turned the wettability of ZnO surfaces from hydrophilic to hydrophobic for some particular applications and needs. For this purpose, different elements are used as dopants or co-dopants of ZnO films such as Na, La, Pb, Mg, (Pb–Mg).[5,19,20] Also, Thirumalai *et al.*[21] reported that bentonite supported Bi_2O_3–ZnO possesses a significant hydrophobicity (a contact angle of 126°) which leads to its self-cleaning property. Additionally, many authors tried to control the morphology of undoped ZnO surface to obtain hydrophobic surfaces or coatings. *I.e.*, control of the self-cleaning property depends on the geometrical structure of film surface. Especially, nanorods and nanowires ZnO array-based films almost are hydrophobic and used as self-cleaning coatings on glass.[22,23] Various techniques have been utilizing to prepare hydrophobic ZnO nanostructured films for self-cleaning application such as magnetron sputtering, spray pyrolysis, thermal oxidation, reactive evaporation, vapor phase epitaxy, electrodeposition, sol–gel, solid-state reaction and, chemical deposition.[23–30] ZnO nanorods[3] and nanodiscs[25] synthesized by a hydrothermal method as well as ZnO nanowires fabricated using thermal evaporation method,[26,27] were reported. ZnO nanowires by long-pulse-width laser ablation (LPLD) was also reported.[28] Similar results were reported for ZnO nanorods[2] and thin films prepared by radio-frequency (RF) magnetron sputtering.[31] However, there is high demand for low cost and massive production of hydrophobic ZnO nanostructured surfaces for many applications such as indoor self-cleaning.

Different techniques have been used to develop ZnO nanostructures such as magnetron sputtering,[31] thermal evaporation,[32] atomic layer deposition,[33] vapor phase epitaxy, solid-state reaction, and hydrothermal method.[34–41] But these techniques required ultra-high vacuum, costly equipment, catalysts, high operation temperatures, or the use of toxic gas compounds. Compared with the previous techniques, controlled fabrication of nanostructured ZnO films by chemical bath deposition (CBD) is smarter because of its excellent features. This is ascribed to its ability to control the morphology and orientation of ZnO by tuning the process parameters.[42] Also, it is inexpensive, simple, rapid, applicable for large scale production, and working under low temperatures (<100 °C) using a variety of substrates.[30] Most of the previous CBD reports mainly focused on the control of the ZnO nanostructures morphology by altering the concentration and temperature of the solution.[43,44]

Successive ionic layer adsorption and reaction (SILAR) has attracted particular interest for preparing the ZnO nanostructure due to its simplicity and low-cost. This is beside its capability to achieve large area coatings and ability to control the morphology of nanostructure.[43,44] Based on the literature survey, there are few reports of nanostructured ZnO thin films prepared by SILAR technique. Also, most of the

previously reported ZnO films by this method were hydrophilic. Additionally, chemical bath deposition (CBD) is more interest because of its excellent characteristics. The CBD can control the orientation and morphology of ZnO by tuning the fabrication parameters.[45] Also, it is a rapid, simple, inexpensive, applicable for large scale production, and working under low temperatures (<100 °C) using a variety of substrates.[46] Most of the previous reports with CBD mainly focused on the control of the ZnO nanomorphology by changing the temperature and concentration of the solution.[47,48] In the present work, the different fabrication parameters of CBD technique will be controlled and optimized to produce hydrophobic ZnO nanostructured coatings on glass substrates coated with seed layer by SILAR technique. In addition, the influences of the deposition time and pH value on the morphological, structural, hydrophobic, and optical properties nanostructured ZnO thin films are reported.

Hydrophobic ZnO nanoarrays have been deposited by several techniques such as pulsed laser deposition,[49] sintering,[50] chemical spray,[51] sol–gel,[52] chemical bath deposition (CBD),[53] a heating reflux,[54] simple successive ionic layer absorption and reaction (SILAR),[55] hydrothermal,[56] and R.F magnetron sputtering.[57]

2   Experimental details

2.1.   Materials

Zinc acetate dihydrate ($Zn(CH_3COOH) \cdot 2H_2O$, ADWIC, 98.5%), citric acid (Fluka, 99.5%), zinc sulphate ($Zn(SO_4)$, Alfa Aesar, 99%), ammonia (NH_4OH, Alfa Aesar), sodium hydroxide (NaOH, Alfa Aeasar, 99.6%), hexamethylene tetra-ammine ($C_6H_{12}N_4$ (HMT), ADWIC, 99%), and hydrochloric acid (HCl, Alfa Aesar, 98%) were used as received from the supplier.
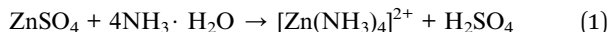
2.2.   Deposition of ZnO nano-seeds layer

To grow well-nanostructured ZnO thin films, first, a nanostructured ZnO seed layer film was deposited on glass substrates using SILAR method. This ZnO-coated substrate is then used for growing ZnO NRs by using CBD method. It is a very simple and relatively cost-effective method for preparing films of any preferred composition under controlled conditions.
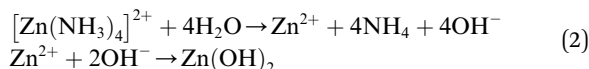
Before use, the glass substrates were washed for 45 min in boiled dilute sulfuric acid (1 : 10 v/v) and then thoroughly rinsed in ethanol, acetone, and deionized (DI) water subsequently. Analytical reagents of $ZnSO_4$ were dissolved in diluted ammonia to obtain a zinc ammonium complex solution. This solution was then served as a cationic precursor. Double distilled water (DDW) kept at 80 °C was used as an anionic precursor. The SILAR growth is a four step process involving subsequent immersion of cleaned glass substrate in cationic and anionic solution along with rinsing the substrate in between in DDW kept at room temperature. In the first step, the substrate was immersed in a beaker containing $Zn(SO_4)$ and ammonia solution for 40 s, where Zn^{2+} with ammonia formed

Paper

zinc ammonia complex ($[Zn(NH_3)_4]^{2+}$) which adsorbed onto the glass substrate, eqn (1).

$$ZnSO_4 + 4NH_3 \cdot H_2O \rightarrow [Zn(NH_3)_4]^{2+} + H_2SO_4 \qquad (1)$$

In the second step, the zinc ammonia adsorbed substrate was immersed into a beaker containing DDW for 20 s. As a result, the adsorbed zinc ammonia complex was converted into zinc hydroxide ($Zn(OH)_2$); eqn (2).

$$[Zn(NH_3)_4]^{2+} + 4H_2O \rightarrow Zn^{2+} + 4NH_4 + 4OH^-$$
$$Zn^{2+} + 2OH^- \rightarrow Zn(OH)_2 \qquad (2)$$

As a third step, the $Zn(OH)_2$ coated substrate was imperiled for 60 s to ultrasonic agitation for removing loosely bonded zinc hydroxide ($Zn(OH)_2$) molecules. Finally, the zinc hydroxide coated substrate was immersed in the DDW bath which was kept at 80 °C for 20 s to convert $Zn(OH)_2$ to solid ZnO film, eqn (3).

$$Zn(OH)_2 \rightarrow ZnO(s) + H_2O \qquad (3)$$

The film was dried for 15 s before the repeating of the deposition cycle. The as-prepared ZnO seed layer films were subjected to annealing at 300 °C for 1 h. The ZnO seed layer films were prepared at 20 cycles.

2.3. Growth of hierarchical ZnO nanostructure thin films

The deposition of hierarchical ZnO nanostructured films onto seed layer films were carried out by using simple chemical bath deposition (CBD) method. All the chemicals were purchased from Aldrich Chemical Corporation and used without further purification. The chemical bath was prepared by mixing equi-molar (0.05 M) aqueous solution of zinc acetate dihydrate $Zn(CH_3COOH) \cdot 2H_2O$ and hexamethylene tetra-ammine (HMT) were dissolved in 20 ml of DI water. When these two compounds were mixed, no precipitation was observed. Finally, white precipitation was observed after continued stirring for 20 min. The pH of the reaction was controlled at 4, 5, 6, 7, and 8 by adding a 0.1 M sodium hydroxide (NaOH) or 0.1 M hydro-chloric acid (HCl) solution. After successful completion of deposition condition, the temperature of the water bath was allowed to cool down to ambient temperature. Finally, the deposited films were removed from the aqueous solution and cleaned carefully with DI water and acetone for several times to remove residual salts and then dried at room temperature for further characterization.

2.4. Samples characterization

X-ray diffraction (XRD, High-resolution Philips X'PertPRO MRD) was used to identify the crystallographic properties of the prepared ZnO films using Cu Kα radiation ($\lambda = 1.5418$ Å) with a step 0.02. The chemical compositional was analyzed using energy dispersive X-ray (EDX; Oxford Link ISIS 300 EDX). Morphological studies of the fabricated nanostructured films were carried out using field emission-scanning electron microscopy, FE-SEM (model: ZEISS SUPRA 55 VP and ZEISS LEO, Gemini Column). Optical spectra in the spectral range 300–1000 nm were measured using UV/VIS/NIR 3700 double beam Shimadzu spectrophotometer at RT. The surface wetta-bility of ZnO thin films was identified by measuring the water contact angle, WCA(Θ). WCA was measured using the sessile drop method by a CAM 200 Optical Contact Angle Meter (KSV Instruments). A 5 µl droplet of deionized (DI) water was posi-tioned on the surface of the sample by a microsyringe. The image of the droplet was captured to measure the angle that formed at the liquid/solid interface. The WCA was measured three times for each sample and the average value was calculated.

3 Results and discussion

3.1. Structural studies

The XRD patterns of ZnO nanostructured films grown at various deposition time, t_D, from 2 to 12 h are shown in Fig. 1. All films exhibit polycrystalline structures. All the peaks are for the
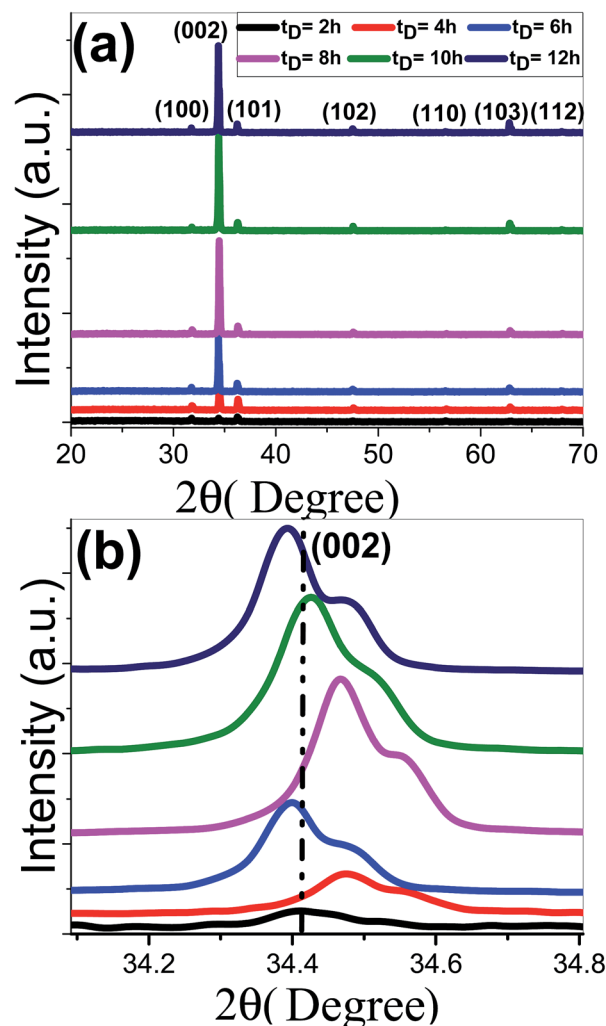

Fig. 1 (a) XRD spectra of nanostructured ZnO films deposited at different deposition times and (b) the (002) peak shift.

hexagonal wurtzite ZnO and space group $C_{6V} = P6_3mc$ (JCPDS-89-0510).[58,59] All films show a strong (0 0 2) diffraction peak at 34.40° and grow preferentially perpendicular to the substrate surface along c-axis. There are other weak peaks at 31.72°, and 36.21°, 47.45°, 56.58°, 62.89°, and 67.86° correspond to (1 0 0), (1 0 1), (1 0 2), (1 1 0), (1 0 3) and (1 1 2) orientation planes of ZnO. No additional impurity phases or metallic Zn phases are detected, which indicates the formation of pure crystalline ZnO films at the relatively lower time of 2 h and the precursors were completely transformed into ZnO phase. With the increase of deposition time till 8 h, the (0 0 2) peaks became stronger and sharper that demonstrated the better growth and crystallization of ZnO thin films. With increasing the deposition time $t_D \geq$ 10 h, the intensity along (0 0 2) direction is decreased.

Fig. 1(b) reveals that the (002) peak position of ZnO samples that deposited at 6 and 12 h has been slightly shifted to lower 2θ values. However, the other samples show a shift to higher 2θ values, which revealed that the inter-planar distance between the (002) planes was decreased and better crystallinity was achieved. For 6 and 12 h, the shift in peak position to lower 2θ values refers to the increase of the inter-planar distance between the (002) planes due to the different strain levels in both samples and indicates the expansion of the lattice parameters.[60] According to Bragg's law:

$$m\lambda = 2d \sin \theta, \tag{4}$$

where d is the inter-planar spacing, λ is the wavelength of the used X-ray, and m is the diffraction order. A rise in "d" leads to a fall in 2θ. Consequently, a variation of deposition time leads to a shift of the characteristic (002) peak to lower or higher angles, which affect the lattice parameters and the volume of the unit cell of the ZnO films. Our results, therefore, indicate that the used technique is an efficient method to get ZnO films free from impurity phases. XRD analysis detects no secondary phases, but the existence of secondary phases cannot be entirely excluded because of the limitations of the XRD characterization technique.[61]

The texture of a particular plane is represented by the texture coefficient (TC). If TC > 1, this refers to the preferred growth. TC is given as:[19,62]

$$TC(hkl) = \frac{I(hkl)/I_o(hkl)}{N^{-1} \sum_n I(hkl)/I_o(hkl)}, \tag{5}$$

where $I(hkl)$ and $I_o(hkl)$ are the measured relative intensity and JCPDS standard intensity, respectively, of a plane (hkl), N is the reflection number, and n is the number of diffraction peaks. TCs values were calculated for the first three main peaks in the XRD patterns. The values for (100), (002) and (101) are presented in Table 1. The entire ZnO films exhibit enhanced intensities corresponding to (002) peak when compared to (100) and (101) peaks. This indicates a preferential orientation along the c-axis, which is associated with the minimum value of the (002) surface free energy. The lowest three densities of the surface free energy are 20.9, 12.3 and 9.9 eV nm^{-2} for (100), (110), and (002) plans, respectively.[63] TC (002) of ZnO is increased by increasing the deposition time till 8 h and then decreased. Increasing deposition time always encourage the growth of ZnO crystallites in the (002) direction, and the highest TC (002) value of 5.6 is obtained for ZnO that fabricated at 8 h. This highly c-axis preferred orientation is critical for piezoelectric applications, $i.e.$ ultrasonic oscillators and transducer devices.[64]

The crystallite size (D) of the ZnO films was determined from the full width at half maximum intensity (FWHM), β, of the first three peaks; (100), (002) and (101), using the well known Scherer's formula, $D = 0.9\lambda/\beta \cos \theta$, where $\lambda = 1.54$ Å. The obtained values of D for the different deposition times are listed in Table 1. The D value of ZnO films is increased from 47.7 to 68.43 nm for $t_D \leq 8$ h and decreased to ~63.4 nm at 10 h. With increasing deposition time, the smaller crystallites in size are aggregated and the highest crystalline quality of ZnO films could be obtained at 8 h.

Using the crystallographic plane indices (h, k, and l), the lattice constants (a and c) of the ZnO films are calculated by using the following equations:[19,65]

$$d_{(h k l)} = \left[\frac{4}{3} \left(\frac{h^2 + k^2 + hk}{a^2} \right) + \frac{l^2}{c^2} \right]^{-0.5} \Rightarrow$$

$$d_{(0 0 2)} = \frac{c}{2} \quad \text{and} \quad d_{(1 0 1)} = \left[\frac{4}{3} \left(\frac{1}{a^2} \right) + \frac{1}{c^2} \right]^{-0.5}, \tag{6}$$

Table 1 The XRD data for the ZnO films; the texture coefficient (TC), the crystallite size (D), the lattice parameter (a, c and volume of the unit cell V), the Zn–O bond length (L), u parameter, and the in-plane stress ($\mathcal{O}$)

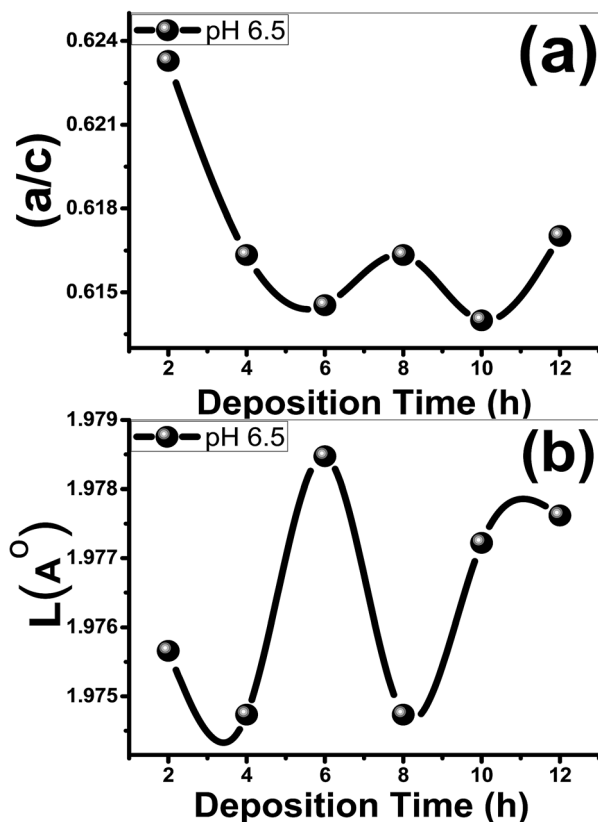| Deposition time/pH		TC (hkl) of ZnO			D (nm)	δ (nm^{-2}) $\times 10^{-4}$	Lattice parameters					$\mathcal{O}$ $\times 10^9$ (N m^{-2})
		(100)	(002)	(101)			a (Å)	c (Å)	V (Å^3)	L (Å)	U	
Deposition time effect@pH 6.5	2 h	1.1	1.6	0.98	47.7	4.40	3.2459	5.2078	47.5176	1.9757	0.37936	−0.20910
	4 h	0.5	3.8	0.8	49.7	4.05	3.2327	5.2450	47.4674	1.9747	0.3765	−3.42469
	6 h	0.31	5.1	0.32	63.2	2.50	3.2357	5.2653	47.7392	1.9785	0.37576	−5.17566
	8 h	0.17	5.6	0.2	68.43	2.14	3.2327	5.2450	47.4674	1.9747	0.3765	−3.42469
	10 h	0.12	5.1	0.2	63.4	2.49	3.2327	5.2651	47.6488	1.9772	0.37554	−5.15781
	12 h	0.18	4.85	0.2	65.6	2.32	3.2386	5.2488	47.6748	1.9776	0.37678	−3.74764
pH effect@8 h	5.5	1.004	0.910	1.084	41.41	5.83	3.2357	5.2281	47.4020	1.9739	0.37755	−1.96061
	6	0.52	2.07	0.40	47.26	4.48	3.2327	5.2826	47.8073	1.9794	0.37471	−6.6713
	7	0.18	3.84	0.43	68.43	2.14	3.2342	5.2739	47.7731	1.9789	0.37523	−5.92112
	8	0.6	3.25	0.58	58.87	2.89	3.2357	5.2479	47.5820	1.9763	0.37659	−3.67693

Fig. 2 (a) The (a/c) ratio and (b) the bond length, L (Å) of the films as a function of the deposition time.

The volume of the unit cell, internal parameter, and Zn–O bond length (V, u and L) of the hexagonal ZnO are calculated using the following equations:[20,66]

$$V = \frac{\sqrt{3}}{2}a^2c \qquad (7)$$

$$u = \left(\frac{1}{3}\right)\left(\frac{a^2}{c^2}\right) + \frac{1}{4} \qquad (8)$$

$$L = \sqrt{\left(\frac{a^2}{3} + \left(\frac{1}{2} - u\right)^2 c^2\right)} \qquad (9)$$

The in-plane stress for hexagonal ZnO crystallites with a highly c-axis preferred orientation can be determined using the biaxial stress–strain model;[63]

$$\mathcal{O} = 4.5 \times 10^{11} \ \frac{c_o - c}{c_o} \ \text{N m}^{-2}, \qquad (10)$$

where c_o is the corresponding value for bulk ZnO (5.2054 Å). The negative (positive) sign of $\mathcal{O}$ indicates that the stress in the films is compressive (tensile) in nature. The time effect could have induced stress in the film and hence the shift in the diffraction peak. The calculated values of a, c, V, u and $\mathcal{O}$ are listed in Table 1. In addition, the influence of deposition time on the a/c ratio and Zn–O bond length (L) are depicted in Fig. 2. As seen from

Table 1, both the u parameter and the ratio of the lattice parameters a/c are affected by deposition time and exhibit a similar behavior, where eqn (5) shows that u is proportional to $(a/c)^2$. The V value of the ZnO film@2 h is 47.5176 Å^3. Then, the V value of the ZnO film is increased from 47.4674 to 47.6748 Å^3 with increasing the deposition time from 8 to 12 h. The same behavior can be observed for the Zn–O bond length, Fig. 2(b). L is altered between 1.97473 and 1.97847 Å, which estimated for the ZnO film that deposited for 6 h. Also, L increases from 1.9747 to 1.9776 Å with increasing deposition time from 8 to 12 h. Also, the value of the stress is changed from 2.09098×10^8 to 51.7566×10^8 N m^{-2} as the deposition time increased from 2 to 6 h. The negative sign of the estimated stress values, Table 1, for the deposited films indicate that the crystallites are under a state of compressive stress that are appearing in all films.

Fig. 3(a) shows the XRD patterns of ZnO nanostructured films deposited at varies pH values. It is noted that all the films exhibit polycrystalline structures with similar features as XRD patterns of Fig. 1(a).[57,58]

No phases related to metallic Zn or Zn compounds are observed at $5.5 \leq \text{pH} \leq 8$. This means that the change of pH values did not change the hexagonal structure of the ZnO films and the precursors were completely transformed into ZnO phase. At pH 5.5, the pattern shows sharper (100), (002), and (101) peaks with TC values of 1.004, 0.910, and 1.084, respectively. The lower values of texture coefficient reveal that the
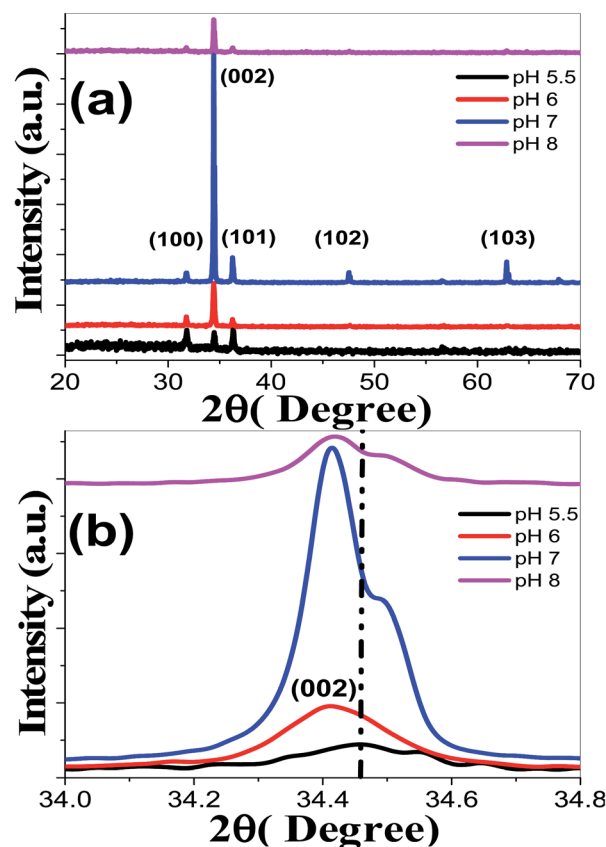

Fig. 3 (a) XRD spectra of nanostructured ZnO films deposited at different pH values and (b) the (002) peak shift.

films have reasonable crystallinity, almost, without preferential orientations. With the increase of pH to 7, the (0 0 2) peaks became stronger and sharper that demonstrated the better growth and crystallization of ZnO thin films. For pH > 7, it was observed that there is a decrease in intensity along (0 0 2) direction. Fig. 3(b) reveals that the (002) peak position of ZnO has been slightly shifted to lower 2θ values by increasing pH value. Consequently, the increase of pH value leads to a shift of the characteristic peaks to lower angles and increase of the interplanar distance according to Bragg's law. Anandan and Muthukumaran[67] reported (002) peak shift to lower 2θ values for the sol–gel prepared Y-doped ZnO nanopowder. Our results, therefore, indicate that our fabrication approach is an efficient method to get ZnO films free from impurity phases.

TCs values at different pH values were calculated using eqn (5) for the first three main peaks ((100), (002) and (101)) and presented in Table 1. The entire ZnO films exhibit enhanced intensities corresponding to (002) peak when compared to (100) and (101) peaks, which indicates a preferential orientation along the c-axis for TC (002) > 1 at 5.5 < pH ≤ 8. This is associated with the minimum value of the (002) surface free energy,

which leads to increased number of grains along this plane.[68] Then, increasing pH to 7 always encourage the growth of ZnO crystallites in the (002) direction, and the highest TC (002) value of 3.84 is achieved at pH 7. Similar results have been reported for Er, La and Yb-doped ZnO nanocrystals.[69] This (002) preferred orientation, highly c-axis, is critical for ultrasonic oscillators and transducer devices.[64]

From Scherer's formula, the crystallite size (D) is increased from 41.41 to 68.43 nm by increasing pH from 5.5 to 7, then it decreases to 58.87 at pH 8, as shown in Table 1. Also, the values of a, c, V, u and $\varnothing$ are calculated and listed in Table 1. In addition, the influence of pH on the a/c ratio and Zn–O bond length (L) are depicted in Fig. 4.

As seen from Table 1, both u parameter and the ratio a/c of the lattice parameters are affected by pH and exhibit a similar behavior. The V value of the nanostructured ZnO film is 47.4020 Å^3@pH 5.5 and increased to 47.8073 Å^3 with increasing pH to 6, and then decreased to 47.582 Å^3 with the further increase of pH to 8. At pH 6, L increases to 1.9794 Å compared to 1.9739 Å@pH 5.5 and then decreases to 1.9763 Å@pH 8, Fig. 4(b). Also, the value of the stress is increased from 1.9606×10^9@pH 5.5 to 6.6713×10^9 N m^{-2}@pH 6 and then decreased to 3.67693×10^9 N m^{-2}@pH 8. Additionally, the negative sign of the estimated stress values, Table 1, for the films indicates that the crystallites of all films are under a state of compressive stress.
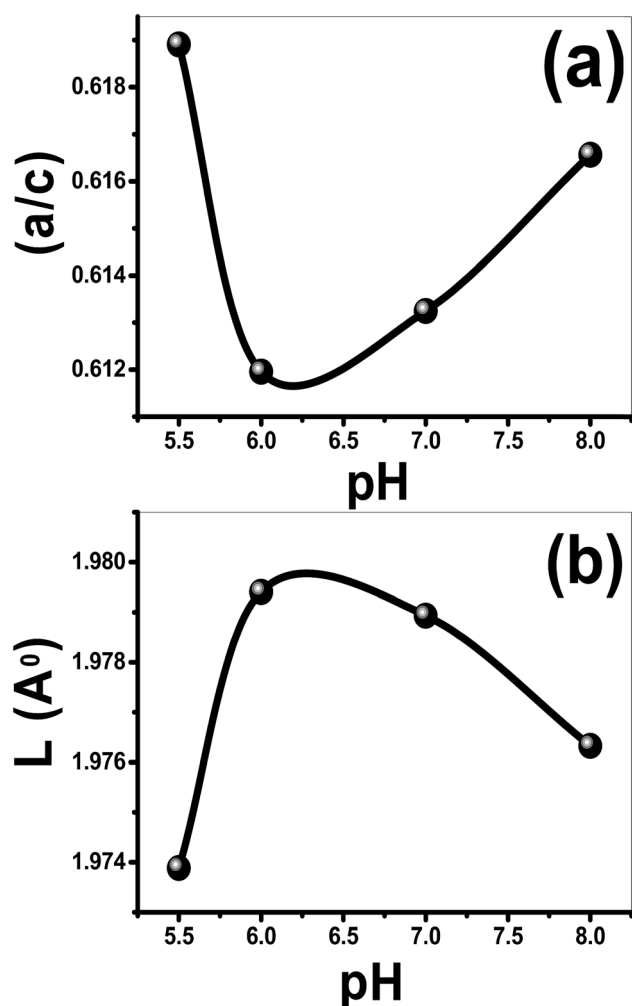

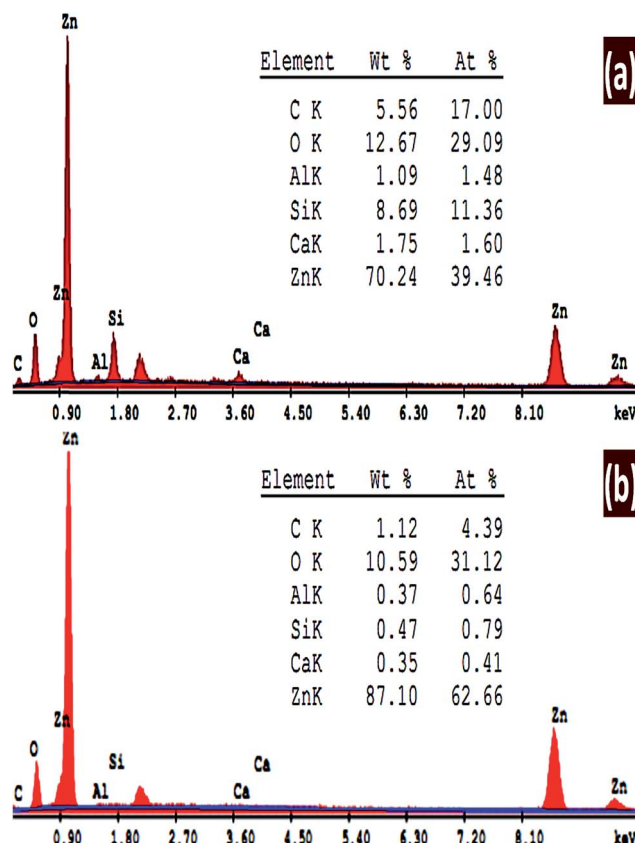Fig. 4 (a) The a/c ratio and (b) the bond length, L (Å), of the films as a function of the pH value.

Fig. 5 EDX spectra of ZnO nanostructured films deposited at 8 h and pH (a) 6.5 and (b) pH 7.

From the previous results, it can be concluded that a proper deposition time and pH can significantly improve the crystalline quality of nanostructured ZnO thin films. This may be interpreted in terms of the decrease in surface energy as the ZnO atoms are trapped at or migrate down the grain boundaries.[70]

3.2. Chemical composition

SEM/EDX spectroscopy is the best widely-used of the surface analytical techniques since it is inexpensive, relatively rapid, and basically a non-destructive approach to surface analysis. The analysis of the emitted EDX signals from the samples gives the quantitative elemental information. Fig. 5 shows the energy dispersive X-ray (EDX) spectra of ZnO nanostructures deposited at 8 h and (a) pH 6.5 and (b) pH 7. The quantitative analyses of the chemical composition of the fabricated ZnO thin films are shown in the inset tables. The EDX spectra clearly confirm the presence of Zn and O peaks. There are three peaks relevant to Zn at around 1, 8.6, and 9.6 keV. In addition, Si, Ca, and Al signals are detected from the glass substrate in the EDX pattern. This is because EDX has a larger interaction volume than the thickness of the ZnO film. As the pH value is increased from 6.5 to 7, almost all the traces signal from the substrate disappeared. The quantitative analysis of the ZnO at pH 6.5 is 84.7% Zn and 15.3% O, which indicates the high purity of the fabricated ZnO thin film. Also, these ratios are very close to the ideal stoichiometric ratio between Zn and O atoms. By increasing pH to 7, the Zn/O ratio is increased as the pH value increased to 7. Therefore; the chart in Fig. 5(a) shows that the O signal not only comes from the ZnO thin film but also from the glass substrate.

3.3. Surface morphological analysis

Fig. 6 shows SEM images of ZnO thin films grown on ZnO seed layer by chemical bath deposition technique with different reaction time: (a) 2, (b) 4, (c) 6, (d) 8, (e) 10, and (f) 12 h. As shown, ZnO nanostructures undergo a gradual morphological evolution with reaction time.

When the deposition has been performed for 2 h, Fig. 6(a), nanorods of random distribution was formed. The disordered growth of ZnO nanorods is due to the nature of the polycrystalline glass substrate. All of the ZnO nanorods display a perfect hexagonal shape throughout their lengths as shown in the SEM image and grow preferentially along the c-axis direction. These nanorods displayed average diameter and length of ~200 and 600 nm, respectively.

Fig. 6(b) displays SEM image of ZnO nanostructured film grown-up for 4 h. A random distribution of hexagonal nanodiscs was formed and accompanied with a few numbers of ZnO nanorods distributed in the ZnO film. The nanorods have average diameter 400 nm and average length 480 nm. The morphology study of the grown ZnO film for 6 h, Fig. 1(c), shows a high density of hexagonal nanodisc formed with a very small number ZnO nanorods spread on the film surface. The ZnO nanodisc takes different and random directions. As the deposition time is prolonged to 8 h, some cracks appear and the number of nanodiscs increase. Then, the simultaneous growth of an enormous number

of nanodiscs limits their sizes and leads to strong interfere between these nanodiscs. Also, the nanorods are disappeared at the longer deposition time, Fig. 1(d). The SEM images 1(a–c) clearly refer to the decrease of the ZnO nanorods density and the complete conversion from hexagonal nanorods into hexagonal nanodisc as the growth time increases. I. e., nanorods numbers decrease and numbers of nanodiscs increase as the time of deposition increased. For $t_D > 8$ h, Fig. 1(e and f), the density and surface area of the hexagonal nanodiscs is increased as the deposition time increased. As the deposition time increased, the discs become thin and interfere with each other. Also, the homogeneity of the film is improved due to the uniform agglomeration of the discs which agrees well with the decrease of the stress values as depicts from XRD calculations Table 1. In addition, the increase of surface area of the hexagonal discs as the deposition time increased is consistent with XRD results that revealed the growth of the crystallite size from 63.4 to 65.6 nm with increasing deposition time from 10 to 12 h. One of the important notes is that the measured sizes by FE-SEM appear to be greater than that calculated by XRD. This suggests that FE-SEM gives the rod or disc size that may be consisted of more than one crystallite, while the XRD gives the crystallite size.

Fig. 7 shows the variation of the film thickness in μm with the deposition time. As shown there are three regimes for the
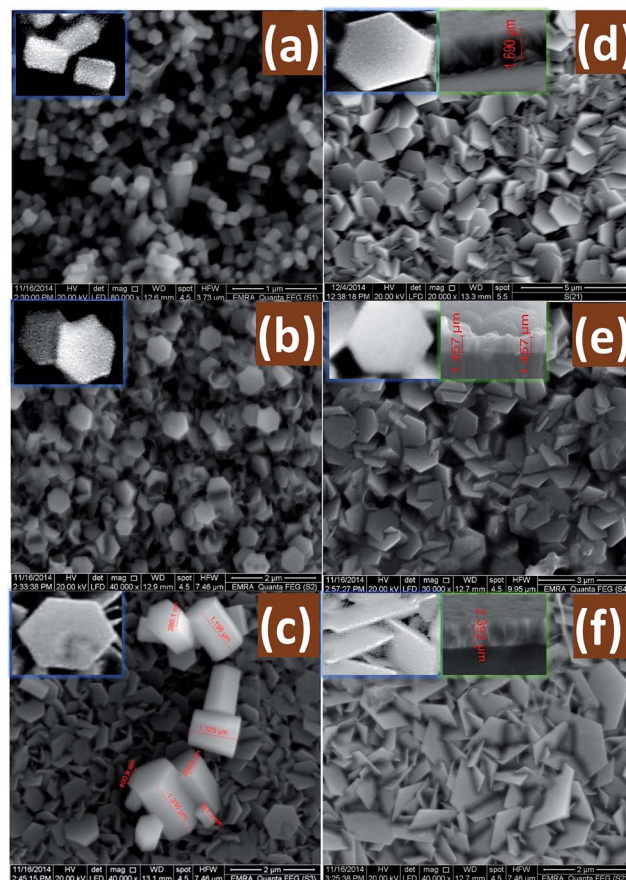

Fig. 6 SEM images of nanostructured ZnO thin films deposited at different times (a) 2, (b) 4, (c) 6, (d) 8, (e) 10 and (f) 12 h. The insets showed magnified and cross-sectional SEM images.
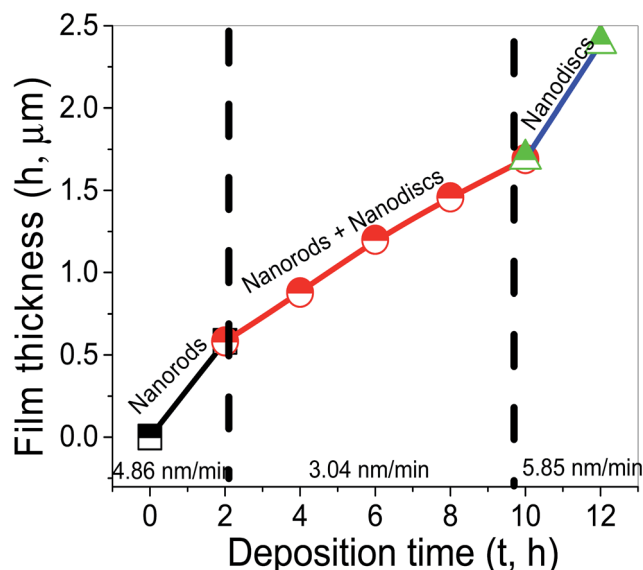
Fig. 7 Variation of film thickness with deposition time.

increase of the film thickness. The thickness of the samples was increased from 582.8 nm at 2 h to 1.4 μm at 8 h and 2.392 μm at 12 h. Then, the vertical growth rate is decreased from 4.86 nm min^{-1} at 2 h to ~3.04 nm min^{-1} at 8 h, and then increased again to 5.85 nm min^{-1} as the growth time increased from 8 to 12 h.

The same result was obtained in a previous study by growing the concentration of OH$^-$ in the precursor.[65] When the OH$^-$ concentration is low, the crystal growth rate along the c axis is faster than the growth rate alongside any other direction. Therefore, the ZnO sample shows the morphology of one-dimensional nanorods. At high OH$^-$ concentrations in the precursor, the (001) surfaces of ZnO with tetrahedral zincs, usually, have terminal OH$^-$ ligands in solution.[71,72] These ligands will prevent the newly produced ZnO clusters from the effective progression on the ZnO crystallites. Therefore, the crystal growth of the ZnO crystallites along the c axis is partially suppressed under this condition. However, they can still grow sideways and finally two-dimensional ZnO nanoplates are formed. In our experiment, ammonia reacts with water to produce ammonium hydroxide, which provides a continuous source of OH$^-$ for hydrolysis. Then, the concentration of OH$^-$ in the solution is increased as the growth time increased. Hence, the hexagonal nanorods (Fig. 1(a)) are converted into hexagonal nanodisc (Fig. 1(c)). These results revealed that the growth duration plays an important role in the morphology of the ZnO nanostructures. The ZnO nanorod size increases and the nanorods densities decrease when increasing the deposition time due to the Ostwald ripening.[73]

Fig. 8 shows FE-SEM images of ZnO nanostructured films deposited at pH 5.5, 6, 7, and 8 for 8 h. As it can be seen, the film deposited at pH 5.5 revealed well-defined morphology with stacked hexagonal slices or plate-like structures. Fig. 8(b) shows hexagonal plates with a random distribution of flower-like structure made up of the submicron rod-like structure. At pH 7, the morphology of the deposited ZnO film, Fig. 8(c), is almost
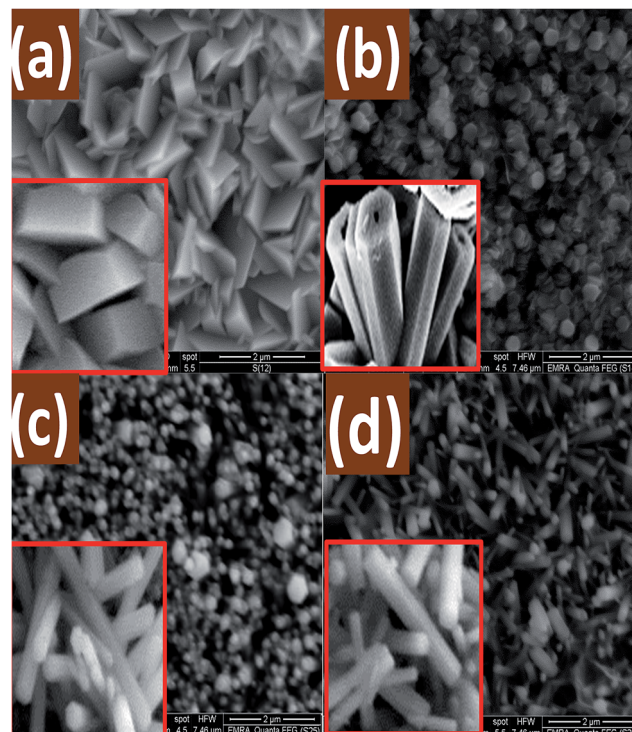

Fig. 8 FE-SEM micrographs for nanostructured ZnO films deposited at different pH values; (a) 5.5, (b) 6, (c) 7, and (d) 8 for 8 h. The insets show corresponding cross-sectional FE-SEM images.

hexagonal nanorods of average diameter 170 nm with a few number of nanodiscs. At pH 8, Fig. 8(d), random distribution of hexagonal nanowires of different diameters is observed and vertically grown from the seeds on the glass substrate. Note that; the nanodiscs are completely disappeared. The length of the nanowires at pH 8 is higher than the length of the nanorods that grown at pH 7. For 9 ≤ pH ≤ 5, the seed layer is etched, and no ZnO nanostructures are grown by this technique.

3.4. Optical properties

3.4.1 Effect of deposition time. UV-vis transmission/absorption spectroscopy is a powerful technique to explore the optical properties and band structure of semiconductor nanomaterials. The transmittance (T%) spectra of ZnO films of different morphologies deposited onto the glass substrates at different deposition time are shown in Fig. 9(A). It is seen, from Fig. 9, that T%, A%, and R% values significantly depend on the film morphology. The nanorods morphology showed the lowest transmission and the highest absorbance and reflection (spectrum a). As the nanodiscs grow at 4 h, the highest transmittance and the lowest absorbance are obtained (spectrum b). By increasing the deposition time, the transmission increased and absorbance decreased. By increasing the wavelength, the reflectance increases and the absorbance almost decreases exponentially.

In most of the visible region of the spectra, T% is increased from 18% to 40% for the four-layered film. However, T% values of 2 layers' film increased from 5% to 10% by increasing the incident wavelength. For wavelength λ > 800 nm, the A% values
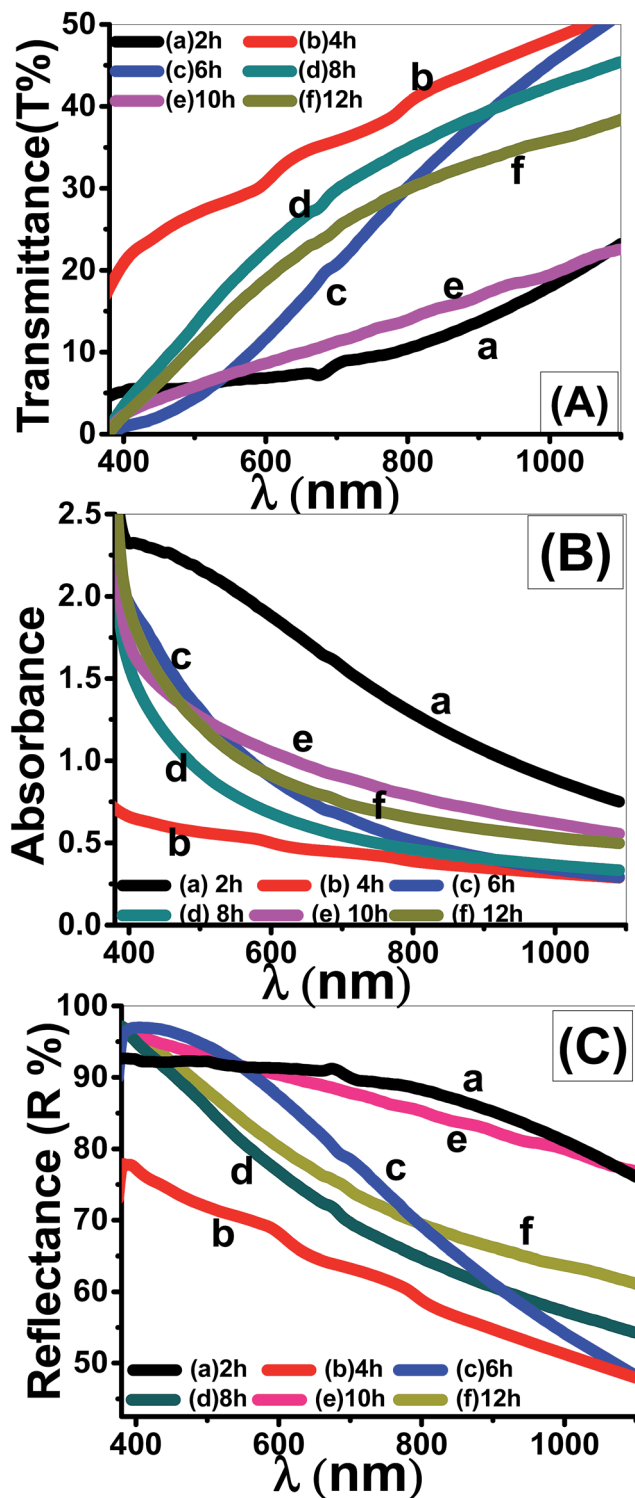
Fig. 9 Optical spectra of nanostructured ZnO thin films deposited at different times; (A) transmittance, (B) absorbance, and (C) reflectance spectra.

of all films that deposited at a time greater than 2 h are smaller and close to zero.[42] Also, it is observed that the absorption edge shifts to longer wavelengths with increasing the deposition time. This observation represents the first indication of the

tuning the optical band gap (E_g) of ZnO films after particular deposition time.

Using the recorded transmission (T) and reflection (R) spectra, the absorption coefficient (α) was calculated using the general expression:[74]

$$\alpha = -\frac{1}{d}\ln\left(\frac{T}{1-R}\right) \qquad (11)$$

where d being the film thickness that measured by FE-SEM images and the values are presented in Fig. 7. The calculated α values were used in the determination of the extinction coefficient ($k = \alpha\lambda/4\pi$) of the films. k reflects the absorption of electromagnetic waves in the semiconductor due to inelastic scattering events.[75] Fig. 10 shows the dependence of k values of the films of a different thickness on the wavelength. As seen, a clear absorption band centered at 355 nm that significantly enhanced and shifted to 365 nm with increasing the deposition time till 6 h, which may be ascribed to the conversion from nanorod to nanodisc morphology. The absorption band shifted to lower wavelength at 8 h, and then shifted to longer wavelengths by increasing the deposition time to 12 h. The k values sharply decrease with increasing λ in the UV region. In the visible region, k values are between 0.02 and 0.07. However, in the region $\lambda > 600$ nm, the k values are very small and constant.

The optical band gap energies can be estimated on according to the following equation, assuming direct transitions between the valence and the conduction bands.[20,76]

$$\alpha E_{photon} = \sqrt{B}\left(E_{photon} - E_g\right)^{1/2}, \qquad (12)$$

where $E_{photon} = h\nu$ is the discrete photon energy and E_g is the band gap energy. B is a temperature independent constant that depends on the refractive index, n_o. B is given by.[77]

$$\sqrt{B} = (4\pi c)\sigma_o/n_o E_U, \qquad (13)$$

where σ_o is the electrical conductivity at the absolute zero and E_U is the Urbach energy. The energy intercept of the plots of
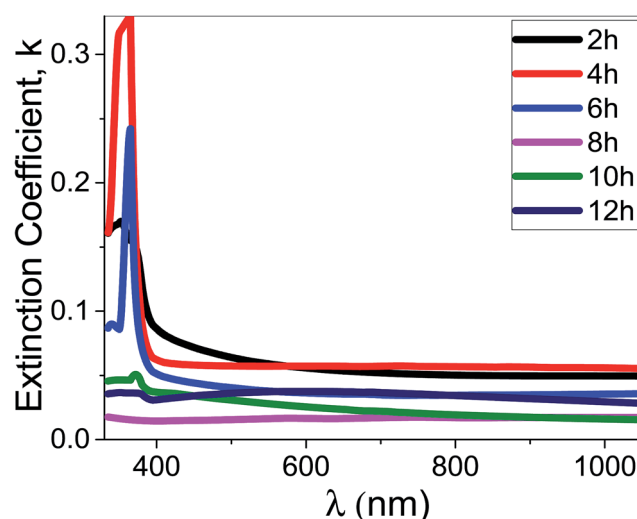

Fig. 10 The extinction coefficient for the synthesized films at different deposition time as a function of the wavelength.

$(\alpha h\nu)^2$ *vs.* $h\nu$ yields E_g for a direct transition, as shown in Fig. 11(a). The corresponding E_g values are listed in Table 2. As seen from Fig. 10(a) and Table 2, the E_g of nanostructured ZnO films is blue shifted from 2.45 to 3.62 eV as the deposition time increased from 2 to 8 h, and then red-shifted to 2.78 eV as the deposition time increased to 12 h. The blue shift may be ascribed to the development of a resonance structure in the density of states, as well as a split-off band by introducing deep states in the band gap.[78] Tuning the E_g values of ZnO films by

controlling the film morphology may, therefore, be used for broadening the optoelectronic and photovoltaic applications of these films.

Urbach energy (E_U) refers to the width of the exponential absorption edge (the tail) and can be calculated by the following relations:[19,79]

$$\alpha = \alpha_o \exp\left(\frac{h\nu}{E_U}\right) \Rightarrow E_U = \left[\frac{d(\ln(\alpha))}{d(h\nu)}\right]^{-1}, \quad (14)$$

where α_0 is the band tailing parameter that can be found by:[19,80]

$$\alpha_o = \sqrt{\frac{\sigma_o\left(\frac{4\pi}{c}\right)}{x\Delta E}}, \quad (15)$$

where σ_o is electrical conductivity at absolute zero, c is the velocity of light, ΔE is the width of the tail of localized states in the forbidden gap. The values of the E_U were obtained from the slopes of the linear fitting of the plots of $\ln(\alpha)$ *versus* $h\nu$, Fig. 11(b). The obtained E_U values are listed in Table 2. E_U increases from 430 to 836 meV as the deposition time increased from 4 to 8 h and then it decreases to 108 meV with the increasing of deposition time to 12 h. The highest E_U, 836 meV, is obtained for the hexagonal nanodisc morphology@8 h, which may be ascribed to the surface roughness and the disorder of the hexagonal morphology of the nanodiscs as shown from SEM image, Fig. 6(d). Also, E_U for the nanorod morphology@2 h is very high, $E_U = 797$ meV. The E_U is attributed to the disorder in the material that leads to the tail in the valence and conduction bands.[81] Therefore, these results confirm the XRD measurements, where the crystalline planes of the ZnO film@2 h shows the lowest preferential orientation along the c-axis (002) direction compared to the other ZnO films.

3.4.2 Effect of pH. Fig. 12 shows optical spectra of nanostructured ZnO films deposited for 8 h at different pH values onto the glass substrates. It is seen that $T\%$, $A\%$, and $R\%$ values significantly depend on the film morphology, pH value, and wavelength of the incident photons. The absorbance and reflectance decrease, whereas the transmittance is increased as the wavelength increased. The stacked hexagonal slices or plate-like structures that grown at pH 5.5 (spectrum a) shows the highest transmission and the lowest reflection. Whereas, the uniform nanorods morphology (spectrum c@pH 7) showed the lowest transmission and the highest absorbance and reflection. The values of transmittance and reflectance of the films that fabricated at pH 6 and 8 are altered between the values of spectra a and c. In most of the visible region, $T\%$ values of the uniform nanorods film are very close to zero and $R\%$ is very close to 97%. At pH 5.5, the absorption edge is located at 365 nm and shifted to 355 nm as the pH increased to 6. The absorption edge of the nanorods morphology that deposited at pH 7 is located at 380 nm and then shifted to 345 nm as the pH increased to 8. This observation represents an indication of the tuning the optical band gap (E_g) of ZnO films after particular pH value.

Using eqn (11), the α values were calculated and used to determine the extinction coefficient ($k = \alpha\lambda/4\pi$) of the films at
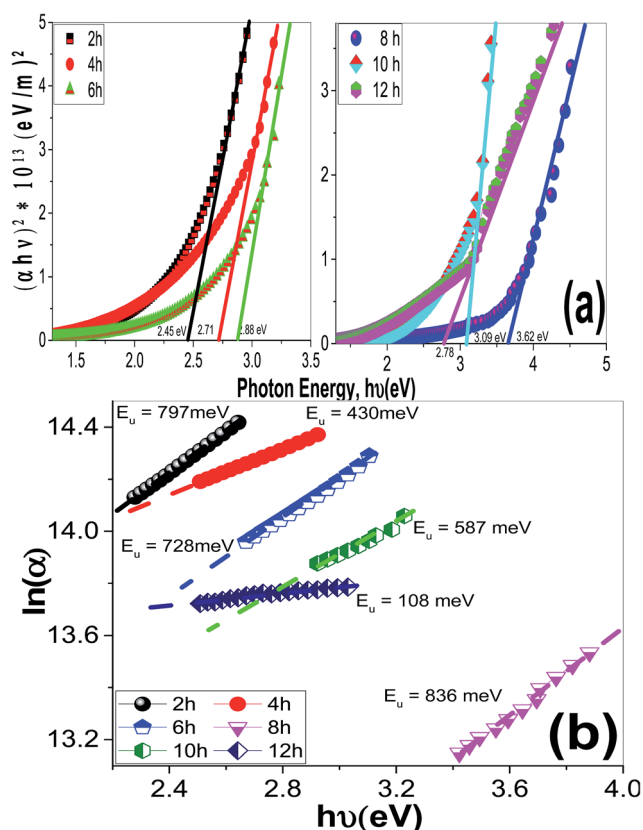

Fig. 11 The plots of (a) $(\alpha h\nu)^2$ & $h\nu$ to determine E_g values and (b) $\ln(\alpha)$ & $h\nu$ to determine to determine the Urbach energy of ZnO films of different morphologies.

Table 2 Optical band gap (E_g), Urbach (E_U) energies, extinction coefficient (k) at 500 nm, and water contact angles, WCA(Θ) of ZnO nanostructured thin films at different deposition time and pH values

Deposition time/pH		E_g (eV)	E_U (meV)	$k@\lambda = 500$ nm	WCA(Θ)
Deposition time effect@pH 6.5	2 h	2.45	797	0.06405	35
	4 h	2.71	430	0.05734	40
	6 h	2.88	728	0.04047	85
	8 h	3.62	836	0.01543	135
	10 h	3.09	587	0.03085	68
	12 h	2.78	108	0.03596	50
pH effect@8 h	5.5	2.72	258	0.04902	30
	6	2.88	828	0.02563	86
	7	3.02	65	0.06243	45
	8	2.78	510	0.03484	23

different pH values. Fig. 13 shows the dependence of k values of the films that fabricated at different pH values on the wavelength. At pH 7, a clear absorption edge is observed at 385 nm, whereas the other films are showed two bands centered at 305 and 360 nm. The band at 305 nm is significantly enhanced as the pH value increased. The k values sharply decrease with
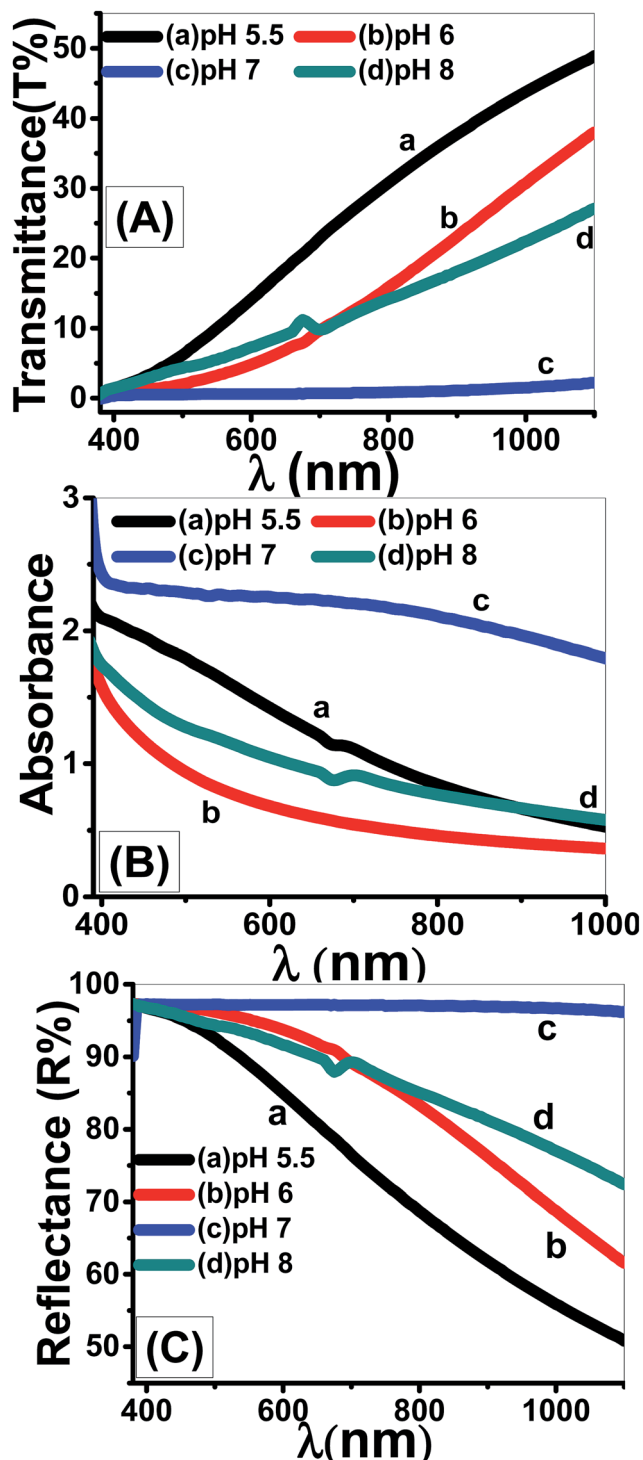

Fig. 12 Optical (A) transmittance, (B) absorbance, and (C) reflectance spectra of nanostructured ZnO thin films fabricated at different pH values.
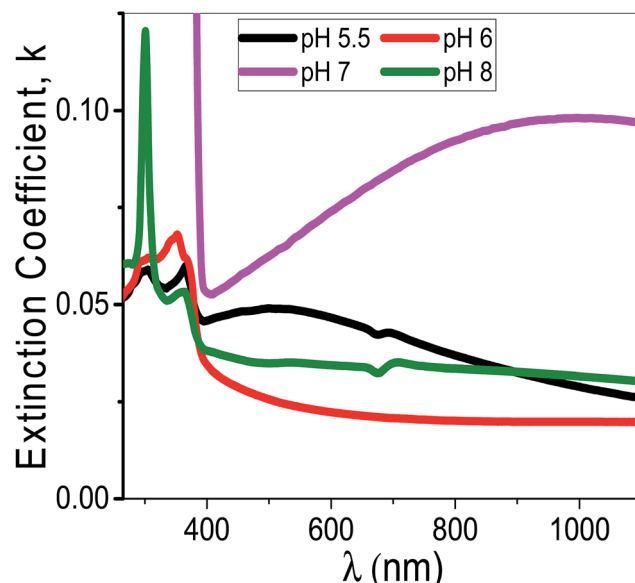

Fig. 13 The extinction coefficient for the synthesized films at different pH values as a function of the wavelength.

increasing λ in the UV region. In the visible region, k values are altered between 0.02 and 0.05 except at pH 7 the k values increased exponentially to 0.1.

Using eqn (12), the energy intercept of the plots of $(\alpha h\nu)^2$ vs. $h\nu$ yields E_g for a direct transition, as shown in Fig. 14(a). The corresponding E_g values at different pH values are listed in Table 2 and plotted in Fig. 14(b) as a function of the pH value. As seen from Fig. 14(b) and Table 2, the E_g of nanostructured ZnO films is blue shifted from 2.72 to 3.62 eV as the pH value increased from 5.5 to 6.5, and then red-shifted to 2.78 eV as the pH value increased to 8. Tuning the E_g values of ZnO films by controlling the pH value and hence the film morphology may, therefore, be used for broadening the optoelectronic and photovoltaic applications of these films.

Fig. 14(c) shows the plots of $\ln(\alpha)$ vs. $h\nu$. The values of the E_U were obtained from the slopes of the linear fitting of this figure. The obtained E_U values are listed in Table 2 and plotted in Fig. 14(d). The minimum E_U, 65 meV is obtained at pH 7 and the maximum value, 836 meV, is obtained at pH 6.5. The E_U is attributed to the disorder in the material that leads to the tail in the valence and conduction bands.[81] Therefore, this is consistent with the XRD results, where the crystallinity enhancement is related to the decrease in the defects and charge carriers and vice versa.[72] Also, this is consistent with the highly ordered nanorods morphology that obtained at pH 7.

3.5. Contact angle measurements

Wettability is a very important property governed by the geometrical structure and chemical composition of solid surfaces.[82,83] However, to fully utilize the hydrophobic properties of nanostructured surfaces, it is necessary to study the fundamental relationship between the different nanostructure and the hydrophobic behavior.
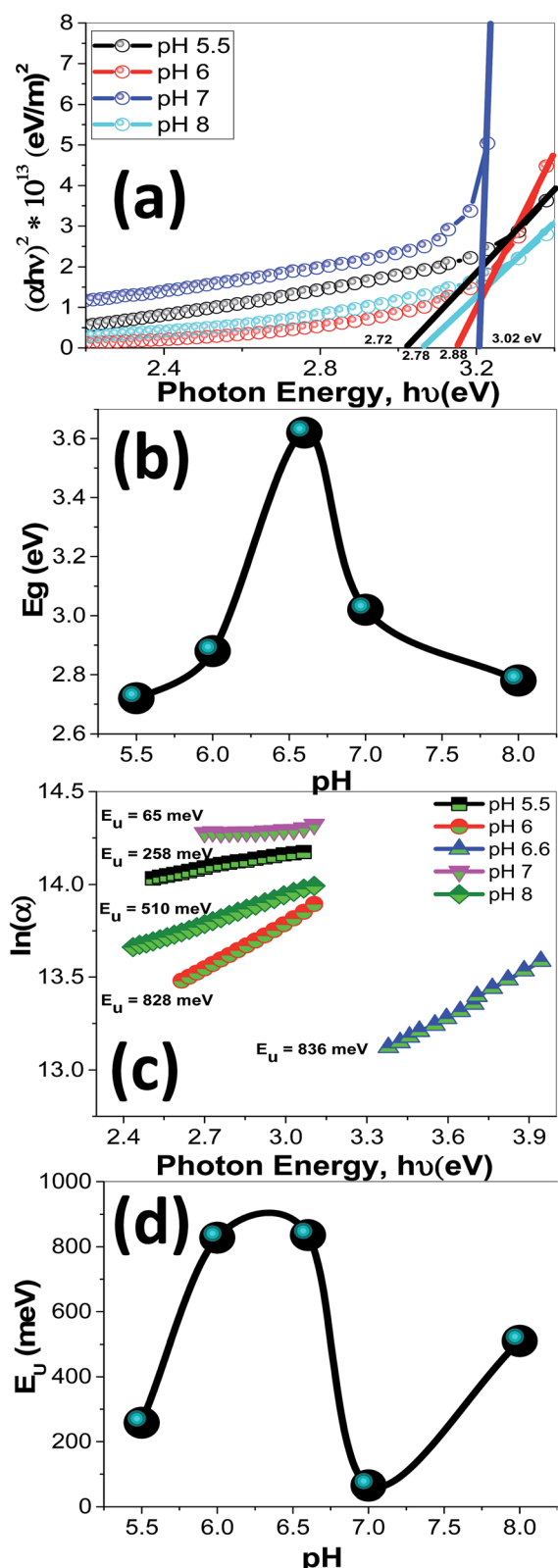
Fig. 14 The plots of (a) $(\alpha h\nu)^2$ & $h\nu$ to determine E_g values, (b) E_g as a function of pH, (c) $\ln(\alpha)$ & $h\nu$ to determine Urbach energy (E_U), and (d) E_U as a function of pH for nanostructured ZnO films.

Two theoretical models (Wenzel model and Cassie–Baxter model) form the basic guidelines for the study of the hydrophobic surface.[84,85] For a liquid drop on a solid surface, the contact angle, Θ, is determined by the surface free energies involved:[20]

$$\cos \Theta = (\gamma_{sv} - \gamma_{sl})/\gamma_{lv} \qquad (16)$$

where γ_{sv}, γ_{sl} and γ_{lv} are the (solid/vapor), (solid/liquid), and (liquid/vapor) tensions, respectively. The main feature of the ZnO-based nanostructures is its gradual transition between different hierarchical morphologies, which allows us to investigate the geometrical effects on the wetting behavior of the samples. The static water contact angle (WCA) is measured through sessile drop method. A 5 μl drop of distilled water was position on the surface with micro-syringe. WCAs were measured at five equidistant and images were recorded in each position was averaged. Fig. 15 shows the contact angle photographs of ZnO nanostructured films fabricated at different (a) deposition time and (b) pH values, from which the WCAs have been evaluated. The obtained values are listed in Table 2. It was observed that different hierarchical ZnO films posse different hydrophobicities which usually enhanced surface roughness when the material has a water contact angle greater than 90° in a smooth form. WCA(Θ) is increased from 35° to 135° ± 2 as the deposition time increased from 2 to 8 h and then decreased to 50° with increasing deposition time to 12 h, Fig. 15(a). Also, WCA(Θ) is increased from 30° to 135° ± 2 as the pH value increased from 5.5 to 6.5 and then decreased to 23° with increasing pH value to 8, Fig. 15(b). This decrease or increase in the wettability is purely due to the surface morphology effect in which the air interfaces or grooves between the individual structures can minimize the contact angle. It is already established that the surface roughness and the surface free energy together are the measure of the wettability of a surface. Such roughness is insufficient to form an increased hydrophobic surface because of the high surface polarity that makes the water fill the grooves very easily through capillary action.[86] Then, the hydrophobic ZnO nanostructured film can be fabricated by optimizing the pH value at 6.5 and the deposition time at 8 h, whereas the hydrophilic nanostructured ZnO films can be obtained by increasing pH value to 8.

These results could be ascribed to the crystallinity and microstructural changes that occur by tuning the deposition time and pH value. A high surface energy material directly formed a hydrophilic surface.[82] The three lowest density of the
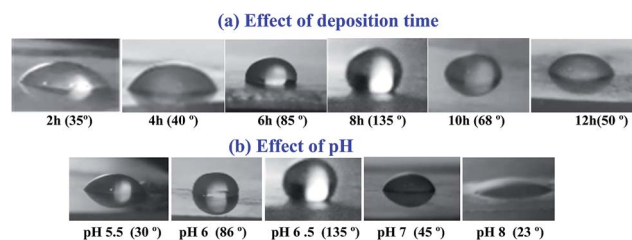

Fig. 15 Contact angles photographs for ZnO nanostructured films fabricated at different (a) deposition time and (b) pH value.

surface free energy is 9.9, 12.3 and 20.9 eV nm^{-2} for (002), (110) and (100) plans, respectively.[87] The preferred orientation along (002) direction seen in ZnO films significantly decreased after 8 h deposition time and pH value 6.5. This means that the crystallinity deterioration leads to increase of the surface free energy of the films at higher pH value and hence reducing Θ values. Moreover, it was reported that the wettability of a surface can be enhanced by increasing the surface roughness within a special size range because the air trapped between the water droplet and the solid surfaces can minimize the contact angle.[88] This support our data as there are changes in the surface morphology (as seen in Fig. 6 and 8) due to the change of the deposition time and the pH value. Similar results were reported for ZnO nanorods[89] and thin films prepared by radio-frequency (RF) magnetron sputtering.[31]

4 Conclusion

ZnO nanostructured thin films of different morphologies were successfully grown on glass substrates at different conditions by a simple two-step wet chemical method. A low-cost successive ionic layer adsorption and reaction (SILAR) method was used to grow ZnO seed layers at 80 °C. Then, different hierarchical based ZnO nanostructured thin films were deposited onto the ZnO seed layers by chemical bath deposition (CBD). The influence of deposition time (t_D) and pH on the surface morphology, wettability behavior, structural and optical properties of the ZnO nanostructured films were systematically investigated. The structural and morphological properties were studied by X-ray diffraction (XRD) and field emission scanning microscopy (FE-SEM). The optical and wetting properties were investigated by UV-Vis spectrophotometer and water contact angle measurement, respectively. The study of the surface morphology revealed a complex and orientated hierarchical based ZnO nanostructured films with diverse shapes from hexagonal nanorods to hexagonal nanoplates or nanodiscs and even much more complex discs/rods and flower-like shapes by changing deposition time and pH of the precursor. XRD results confirm the synthesis of nanostructured ZnO of the hexagonal structure with a preferential orientation along (002) lattice plane. The average crystallite size, D, is increased from 47.7 to 68.43 nm for $t_D \leq 8$ h and decreased to ~63.4 nm at 10 h. Also, D value is increased from 41.41 to 68.43 nm by increasing pH from 5.5 to 7; then it decreases to 58.87 at pH 8. At pH 6.5, the films are hydrophilic for 10 h $\leq t_D \leq 6$ h and hydrophobic for 6 h $< t_D <$ 10 h. The wetting properties of the films were enhanced by increasing or decreasing pH around 6.5. Morphology and thickness of ZnO nanostructure could efficiently control transmittance, absorbance, optical band gap, and the extinction coefficients of the films. The optical band gap is blue shifted from 2.45 to 3.62 eV, and the contact angle is increased from 35° to 135° ± 2 as the deposition time increased from 2 to 8 h. Also, the Optical band gap is blue shifted from 2.72 to 3.62 eV and contact angle is increased from 30° to 135° ± 2 as the pH value increased from 5.5 to 6.5. The existence of stable hydrophobic zinc oxide nanostructured films at room temperature with large-scale and band gaps around 3.62 eV supports their use in self-cleaning and gas sensing applications.

Notes and references

1 G. Kenanakis, E. Stratakis, K. Vlachou, D. Vernardou, E. Koudoumas and N. Katsarakis, *Appl. Surf. Sci.*, 2008, **254**, 5695–5699.

2 J. Lv, J. Zhu, K. Huang, F. Meng, X. Song and Z. Sun, *Appl. Surf. Sci.*, 2011, **257**, 7534–7538.

3 H. J. Butt, K. Graf and M. Kappl, *Physics and chemistry of interfaces*, Wiley-VCH; John Wiley, distributor, WeinheimChichester, 2nd rev. and enl. edn., 2006, vol. xii, p. 386.

4 M. A. Pietrzyk, E. Zielony, M. Stachowicz, A. Reszka, E. Płaczek-Popko, A. Wierzbicka, E. Przezdziecka, A. Droba and A. Kozanecki, *J. Alloys Compd.*, 2014, **587**, 724–728.

5 P. V. Korake, R. S. Dhabbe, A. N. Kadam, Y. B. Gaikwad and K. M. Garadkar, *J. Photochem. Photobiol., B*, 2014, **130**, 11–19.

6 J. W. Lee, K. N. Hui, K. S. Hui, Y. R. Cho and H. Hwan Chun, *Appl. Surf. Sci.*, 2014, **293**, 55–61.

7 R. Vettumperumal, S. Kalyanaraman and R. Thangavel, *J. Lumin.*, 2015, **158**, 493–500.

8 M. Hjiri, R. Dhahri, K. Omri, L. El Mir, S. G. Leonardi, N. Donato and G. Neri, *Mater. Sci. Semicond. Process.*, 2014, **27**, 319–325.

9 E. Isbilir, Z. Serbetci and M. Soylu, *Superlattices Microstruct.*, 2014, **67**, 144–155.

10 D. Chu, Y. Zeng and D. Jiang, *Mater. Lett.*, 2006, **60**, 2783–2785.

11 S. Iwan, J. L. Zhao, S. T. Tan, S. Bambang, M. Hikam, H. M. Fan and X. W. Sun, *Mater. Sci. Semicond. Process.*, 2015, **30**, 263–266.

12 S. Gowrishankar, L. Balakrishnan and N. Gopalakrishnan, *Ceram. Int.*, 2014, **40**, 2135–2142.

13 Y. C. Lin, C. H. Chang, C. H. Shen, P. W. Wang and Y. C. Lee, *Thin Solid Films*, 2010, **518**, 6055–6060.

14 M. Soylu and O. Savas, *Mater. Sci. Semicond. Process.*, 2015, **29**, 76–82.

15 N. Kiomarsipour and R. S. Razavi, *Ceram. Int.*, 2014, **40**, 11261–11268.

16 L. Y. Lin, H. J. Kim and D. E. Kim, *Appl. Surf. Sci.*, 2008, **254**, 7370–7376.

17 V. Kekkonen, A. Hakola, T. Kajava, E. Sahramo, J. Malm, M. Karppinen and R. H. A. Ras, *Appl. Phys. Lett.*, 2010, **97**, 044102.

18 J. Tam, G. Palumbo and U. Erb, *Materials*, 2016, **9**, 151.

19 M. Shaban and A. M. El Sayed, *Mater. Sci. Semicond. Process.*, 2016, **41**, 323–334.

20 M. Shaban and A. M. El Sayed, *Mater. Sci. Semicond. Process.*, 2015, **39**, 136–147.

21 K. Thirumalai, E. T. D. Kumar, R. Aravindhan, J. R. Rao and M. Swaminathan, *Surfaces and Interfaces*, 2016, **5**, 30–38.

22 O. Akhavan, M. Mehrabian, K. Mirabbaszadeh and R. Azimirad, *J. Phys. D: Appl. Phys.*, 2009, **42**, 225305.

23 P. S. Kumar, J. Sundaramurthy, D. Mangalaraj, D. Nataraj, D. Rajarathnam and M. P. Srinivasan, *J. Colloid Interface Sci.*, 2011, **363**, 51–58.

24 X. W. Sun, J. Z. Huang, J. X. Wang and Z. Xu, *Nano Lett.*, 2008, **8**(4), 1219–1223.

25 V. P. Verma, H. Jeon, S. Hwang, M. Jeon and W. Choi, *IEEE Trans. Nanotechnol.*, 2008, **7**(6), 782–786.

26 Z. Guo, X. Chen, J. Li, J. H. Liu and X. J. Huang, *Langmuir*, 2011, **27**, 6193–6200.

27 J. M. Szarko, J. K. Song, C. W. Blackledge, I. Swart, S. R. Leone, S. Li and Y. Zhao, *Chem. Phys. Lett.*, 2005, **404**, 171–176.

28 J. B. Baxter, A. M. Walker, K. vam Ommering and E. S. Aydil, *Nanotechnology*, 2006, **17**, 304–312.

29 L. Zhang, L. Yin, C. Wang, N. Lun and Y. Qi, *ACS Appl. Mater. Interfaces*, 2010, **2**, 1769–1773.

30 P. Sangpour, M. Roozbehi, O. Akhavan and A. Z. Moshfegh, *Curr. Nanosci.*, 2009, **5**, 479–484.

31 P. W. Chi, C. W. Su, B. H. Jhuo and D. H. Wei, *Int. J. Photoenergy*, 2014, **1–10**, 765209, DOI: 10.1155/2014/765209.

32 M. Reza Khanlary, V. Vahedi and A. Reyhani, *Molecules*, 2012, **17**, 5021–5029.

33 J. Lim and C. Lee, *Thin Solid Films*, 2007, **515**, 3335–3338.

34 L. Armelao, M. Fabrizio, S. Gialanella and F. Zordan, *Thin Solid Films*, 2001, **394**, 89–95.

35 C. Hock Ong, J. Hui Wang, H. Gong and H. S. O. Chan, *Int. J. Mod. Phys. B*, 2002, **16**, 314–321.

36 T. Sisianu, O. Lupan, S. Sisianu, S. Railean and V. Besliu, *Proceedings of the Third International Conference on Microelectronics and Computer Science, 1, ICMCS-2002*, 2002, pp. 292–296.

37 I. Stambolova, K. Konstantinov, S. Vassilev, P. Peshev and T. Tsacheva, *Mater. Chem. Phys.*, 2000, **63**(2), 104–108.

38 D. J. Qiu, H. Z. Wu, A. M. Feng, Y. F. Lao, N. B. Chen and T. N. Xu, *Appl. Surf. Sci.*, 2004, **222**, 263–268.

39 M. Purica, E. Budianu, E. Rusu, M. Danila and R. Gavrila, *Thin Solid Films*, 2002, **403–404**, 485–488.

40 T. P. Niesen and M. R. De Guire, *Solid State Ionics*, 2002, **151**, 61–68.

41 Y. F. Nicolau, *Appl. Surf. Sci.*, 1985, **22–23**, 1061–1074.

42 K. Govender, D. S. Boyle, P. B. Kenway and P. O'Brien, *J. Mater. Chem.*, 2004, **14**, 2575–2591.

43 P. K. Giri, S. Dhara and R. Chakraborty, *Mater. Chem. Phys.*, 2010, **122**, 18–22.

44 H. Zhu, H. Jia, D. Liu, Y. Feng, L. Zhang, B. Lai, T. He, Y. Ma, Y. Wang, J. Yin, Y. Huang and Y. Mai, *Appl. Surf. Sci.*, 2012, **258**, 6018–6023.

45 K. Govender, D. S. Boyle, P. B. Kenway and P. O'Brien, *J. Mater. Chem.*, 2004, **14**, 2575–2591.

46 Y. Liu, X. Chen and J. H. Xin, *Nanotechnology*, 2006, **17**, 3259–3263.

47 W. Zhang, P. Wang, X. Fei, Y. Xiu and G. Jia, *Int. J. Electrochem. Sci.*, 2015, **10**, 4688–4695.

48 F. P. Albores, F. P. Delgado, W. A. Flores, P. A. Madrid, E. R. Valdovinos and M. Yoshida, *J. Nanomater.*, 2011, **643126**, 11.

49 E. L. Papadopouloua, V. Zorbab, A. Pagkozidisa, M. Barberogloua, E. Stratakisa and C. Fotakisa, *Thin Solid Films*, 2009, **518**, 1267–2127.

50 T. Wanga, L. Changa, S. Yanga, Y. Jiaa and C. Wongb, *Ceram. Int.*, 2013, **397**, 8165–8172.

51 R. Mimounia, N. Mahdhib, K. Boubakera, A. Madouric and M. Amloukac, *Superlattices Microstruct.*, 2016, **91**, 345–357.

52 S. Patra, S. Sarkar, S. K. Bera, R. Ghosh and G. K. Paul, *J. Phys. D: Appl. Phys.*, 2009, **42**, 075301.

53 V. R. Shindea, C. D. Lokhandea, R. S. Maneb and S. H. Hanb, *Appl. Surf. Sci.*, 2005, **245**, 407–413.

54 Z. Lia, K. Zhua, Q. Zhaob and A. Mengb, *Appl. Surf. Sci.*, 2016, **377**, 23–29.

55 P. Suresh Kumara, A. Dhayal Raja, D. Mangalarajb and D. Natarajaa, *Thin Solid Films*, 2010, **518**, 183–186.

56 Y. You Wanga, G. Qiang Zhoua, J. Guoa and T. Qing Liua, *Ceram. Int.*, 2016, **42**, 12467–12474.

57 V. Şenaya, S. Patb, Ş. Korkmazb, T. Aydoğmuşb, S. Elmasb, S. Özenb, N. Ekemb and M. Zafer Balbağc, *Appl. Surf. Sci.*, 2014, **318**, 2–5.

58 R. Mariappan, V. Ponnuswamy, P. Suresh, R. Suresh and M. Ragavendar, *Superlattices Microstruct.*, 2013, **59**, 47–59.

59 M. Soylu and O. Savas, *Mater. Sci. Semicond. Process.*, 2015, **29**, 76–82.

60 C. Suryanarayan and M. Grant Norton, *X-Ray Diffraction: A Practical Approach*, Plenum Press, New York, 1998.

61 M. Ashokkumar and S. Muthukumaran, *JOL*, 2014, **145**, 167–174.

62 D. Li, J. Feng Huang, L. Yun Cao, J. Yin Li, H. Boou Yang and C. Yan Yao, *Ceram. Int.*, 2014, **40**, 2647–2653.

63 L. W. Wang, F. Wu, D. X. Tian, W. J. Li, L. Fang, C. Y. Kong and M. Zhou, *J. Alloys Compd.*, 2015, **623**, 367–373.

64 A. Taabouche, A. Bouabellou, F. Kermiche, F. Hanini, Y. Bouachiba, A. Grid and T. Kerdjac, *Mater. Sci. Semicond. Process.*, 2014, **28**, 54–58.

65 M. Shaban, M. Mustafa and A. M. El Sayed, *Mater. Sci. Semicond. Process.*, 2016, **56**, 329–343.

66 J. A. Mary, J. J. Vijaya, J. H. Dai, M. Bououdina, L. J. Kennedy and Y. Song, *Mater. Sci. Semicond. Process.*, 2015, **34**, 27–38.

67 S. Anandan and S. Muthukumaran, *Opt. Mater.*, 2013, **35**, 2241–2249.

68 L. W. Wang, F. Wu, D. X. Tian, W. J. Li, L. Fang, C. Y. Kong and M. Zhou, *J. Alloys Compd.*, 2015, **623**, 367–373.

69 R. Zamiri, A. F. Lemos, A. Reblo, H. A. Ahangar and J. M. F. Ferreira, *Ceram. Int.*, 2014, **40**, 523–529.

70 R. Mimouni, K. Boubaker and M. Amlouk, *J. Alloys Compd.*, 2015, **624**, 189–194.

71 J. Slunec ko, M. Kosec, J. Holc and G. Drazic, *J. Am. Ceram. Soc.*, 1998, **81**, 1121–1124.

72 P. K. Dutta, P. K. Gallagher and J. Twu, *Chem. Mater.*, 1992, **4**, 847–851.

73 O. Krichershy and J. Stavan, *Phys. Rev. Lett.*, 1993, **70**, 1473–1477.

74 Y. Dongliang, G. Chuannan and D. Youwei, *J. Semicond.*, 2009, **30**, 072003.

75 A. M. El Sayeda and M. Shaban, *Spectrochim. Acta, Part A*, 2015, **149**, 638–646.

76 M. Moustafaa, A. Paulheima, M. Mohameda, C. Janowitza and R. Manzkea, *Appl. Surf. Sci.*, 2016, **366**, 397–403.

77 M. S. Jiang, Q. Mei Sui, Z. Wei Jin, F. Y. Zhang and L. Jia, *Optik*, 2014, **125**, 3295–3298.

78 L. Aïnouchea, L. Hamadoua, A. Kadria, N. Benbrahima and D. Bradaib, *Sol. Energy Mater. Sol. Cells*, 2016, **151**, 179–190.

79 R. Mimouni, K. Boubaker and M. Amlouk, *J. Alloys Compd.*, 2015, **624**, 189–194.

80 S. Sharma, S. Vyas, C. Periasamy and P. Chakrabarti, *Superlattices Microstruct.*, 2014, **75**, 378–389.

81 A. M. El Sayed and A. Ibrahim, *Mater. Sci. Semicond. Process.*, 2014, **26**, 320–328.

82 J. Lv, J. Zhu, K. Huang, F. Meng, X. Song and Z. Sun, *Appl. Surf. Sci.*, 2011, **257**, 7534–7538.

83 J. Hu, Y. Sun, W. Zhang, F. Gao, P. Li, D. Jiang and Y. Chen, *Appl. Surf. Sci.*, 2014, **317**, 545–551.

84 R. N. Wenzel, *Ind. Eng. Chem. Res.*, 1936, **28**, 988.

85 A. B. D. Cassie and S. Baxter, *J. Chem. Soc., Faraday Trans.*, 1944, **40**, 546.

86 P. S. Kumar, J. Sundaramurthy, X. Zhang, D. Mangalaraj, V. Thavasi and S. Ramakrishna, *J. Alloys Compd.*, 2013, **553**, 375–382.

87 L. W. Wang, F. Wu, D. X. Tian, W. J. Li, L. Fang, C. Y. Kong and M. Zhou, *J. Alloys Compd.*, 2015, **623**, 367–373.

88 H. Luo, J. Ma, P. Wang, J. Bai and G. Jing, *Appl. Surf. Sci.*, 2015, **347**, 868–874.

89 A. Yumak, G. Turgut, O. Kamoun, H. Ozisik, E. Deligoz, P. Petkova, R. Mimouni, K. Boubaker, M. Amlouk and S. G. Said, *Mater. Sci. Semicond. Process.*, 2015, **39**, 103–111.